

Blind nonlinear unmixing using nonnegative matrix factorization based bi-objective autoencoder

Sreejam Muraleedhara Bhakthan, Agilandeewari Loganathan, Aashish Bansal

School of Information Technology and Engineering, Vellore Institute of Technology (VIT), Vellore, India

Article Info

Article history:

Received Sep 22, 2022

Revised Mar 21, 2023

Accepted Apr 2, 2023

Keywords:

Bi-objective autoencoder
Endmember extraction
Hyperspectral image processing
Hyperspectral unmixing
Nonnegative matrix factorization

ABSTRACT

Hyperspectral image processing is one of the trending techniques used in many fields such as remote sensing, medical, agriculture, food processing, and military. The unique discrimination of hyperspectral images can be used for object identification, classification, and prediction. One of the main challenges of these tasks is the mixed pixel problem. Hyperspectral unmixing is the process of identifying the endmembers and their abundance in pixels. In linear unmixing, the mixture of the endmembers is assumed to be linear homogenous patches. Even though these models are simple and faster in performance, most of the real-world images are not linear. A modified nonlinear mixture-based sparsity regularized bi-objective autoencoder model based on nonnegative matrix factorization (NMF-BOA) is proposed in this article. The performance analysis shows that our model gives competitive results compared to the state-of-the-art models.

This is an open access article under the [CC BY-SA](https://creativecommons.org/licenses/by-sa/4.0/) license.



Corresponding Author:

Agilandeewari Loganathan

School of Information Technology and Engineering, Vellore Institute of Technology (VIT)

632014 Vellore, Tamil Nadu, India

Email: agila.l@vit.ac.in

1. INTRODUCTION

Hyperspectral images have been used in many fields because of their unique discrimination features since they capture information in continuous electromagnetic spectra. The hyperspectral images are captured using special spectral sensors. The images captured contain spectral and spatial information about the object under scrutiny. These images are called hypercubes and are enriched with different spectral-spatial information [1]. The image captured using hyperspectral sensors are usually having low spatial resolution. A single pixel in a hypercube covers a large area on the ground. If the area is covered by a single material, then the pixel will be having a pure signature of that material. Otherwise, spectral signatures of different materials present in the area will be stored in a single pixel. This is called a mixed pixel problem. Different atmospheric conditions, physical phenomena, defects, and errors in the sensors also lead to mixed pixels. Identifying the pure endmembers and their abundance is an important challenge in most of the hyperspectral image analysis processes. The general hyperspectral image analysis includes image acquisition, feature extraction [2], band selection [3], classification [4], [5], and prediction [6] as per various applications [7]. To attain better image classification and prediction, the above said problem of mixed pixels have to be solved by the hyperspectral unmixing process, which decomposes the different endmembers present in pixels with their fractional abundance.

The mixing models are broadly classified into linear mixing models (LMM) and nonlinear mixing models (NLMM) based on pixel distribution. Even though the linear unmixing models are simple and easy to implement, in most real-world scenarios the pixels are intimately or heterogeneously mixed. NMF has been a widely used technique for matrix decomposition. Its special features like nonnegative factorization of inversion

problems and blind source separation have attracted researchers for NMF hyperspectral image unmixing. Lee and Seung [8] introduced NMF in Nature Journal as a dimensionality reduction mechanism. A high-dimensional nonnegative matrix can be decomposed into two nonnegative low-rank matrix factors [9]. Over the years many NMF-based models have been proposed for unmixing [10], [11]. A linear NMF model considering the shadows was proposed by Benhalouche *et al.* [12]. Clustering guided NMF model was proposed in [13] using a self-supervised learning method. Many constrained nonnegative matrix factorization (CNMF) models and regularization-based NMF [14] models have been proposed to solve the constrained unmixing problem. Qu *et al.* [9] proposed $L \frac{1}{2}$ Normalization based geometric and statistical hybrid model. Several total variation-based models were proposed recently [15], [16].

Most of the NMF models do not include spatial information for the unmixing. A new method spectral-spatial weighted sparse NMF (SSWNMF), was proposed in [17]. The NMF model included two weight factors for improving the sparsity using a multiplicative iterative strategy. The model was able to capture the smooth structure of the data. Dong *et al.* [18] offered a novel unmixing model for noisy and missing data was proposed. A spatial-spectral kernel regularizer was used for reducing the noise and completing missing elements. The spatial-spectral neighborhood was preserved by selecting similar pixels in the image using a distance measure. Deep learning based unmixing models are also proposed for unmixing the hyperspectral images. Recently autoencoder-based models are popularly used for unmixing and classification of hyperspectral data. Su *et al.* [19] suggested a stacked and variational autoencoders were used for the unsupervised unmixing. The various popular autoencoder models are, a probability metric-based autoencoder model [20], a sparse autoencoder model [21], and sparsity-based autoencoder with orthogonal sparse prior [22]. In this article, a dual branch autoencoder was proposed to implement this novel orthogonal sparsity-based blind unmixing. A multilayer autoencoder for smoothing the abundance. Spatial and contextual pieces of information were used for tackling the outliers [23].

The main requirements evident from the state-of-the-art models are: i) deep learning-based efficient models are needed for efficient sparsity regularization [17]; ii) unmixing considering spectral-spatial features and regularization is needed; and iii) reducing the complexity of hyperspectral data and selecting appropriate similarity pixels [18].

In this article, a nonlinear mixing model-based NMF model using an autoencoder considering the sparsity and the unmixing constraints is proposed. The nonlinear function is modified to a linear function [24] and the autoencoders are used to update the variables in the NMF. The contributions of our proposed model are:

- A new nonlinear bi-objective autoencoder-based NMF is used for hyperspectral unmixing combining the NMF and deep learning techniques.
- The autoencoder pairs use regularization for both abundance and endmember terms in the objective function.
- Rough set theory-based band selection is used for the dimensionality reduction of the hyperspectral image Jasper ridge which is the commonly used real dataset for the hyperspectral unmixing.

The rest of the article is organized as follows. Section 2 presents a detailed description of the proposed model with the architecture and algorithm. The results obtained and the comparison with the existing methods are given in section 3 titled results and discussion. Section 4 summarizes this article with the conclusion.

2. PROPOSED METHOD

The proposed architecture is given in Figure 1. The first step is the preprocessing of the image. The preprocessing steps are image calibration, band removal, denoising, and normalization. The next step in the proposed model is dimensionality reduction using feature extraction and band selection. In our proposed model, the roughset-based band selection followed by feature extraction using autoencoder is used. After dimensionality reduction, the pixels are unmixed by extracting the endmembers and estimating the corresponding abundance information. The algorithm for the proposed model is given as in algorithm. The rest of the section gives detailed working of each stage in the proposed model.

2.1. Preprocessing

The raw images need to be preprocessed before unmixing and classification process. In this proposed model, the spectral preprocessing stage consists of 4 steps, calibration, band removal, denoising, and normalization. The first step is calibration. The raw hyperspectral image is calibrated by water absorption removal, radiometric correction, and other calibrations using ENVI software. Where I is the image vector, $I=[I_1, I_2, I_3 \dots I_N] \in R^{L \times N}$, L is the number of spectral bands and N is the number of Pixels. The next step is band removal, the high frequency, and low-frequency bands. The different types of noises present in hyperspectral images are Gaussian or white noise, stripe noise, impulse noise or spikes, deadlines, and mixed noise. The hypercube with a reduced number of bands will be denoised using Gaussian filter. The next step is

the normalization of the hyperspectral image. The normalization helps to obtain better saliency features of the hyperspectral images. There are several normalization methods such as max, min, max-min, and Gaussian. In this work, the normalization is done using the (1) and (2).

$$C[i, j] = \sqrt{\frac{\sum_{k=1}^B (I_d[i, j, k])^2}{B}} \quad (1)$$

$$I_n[i, j, k] = \frac{I_d[i, j, k]}{c[i, j]} \quad (2)$$

Where I_d is the hyperspectral image with the dimension $A \times B \times C$ after the denoising and I_n is normalized image.

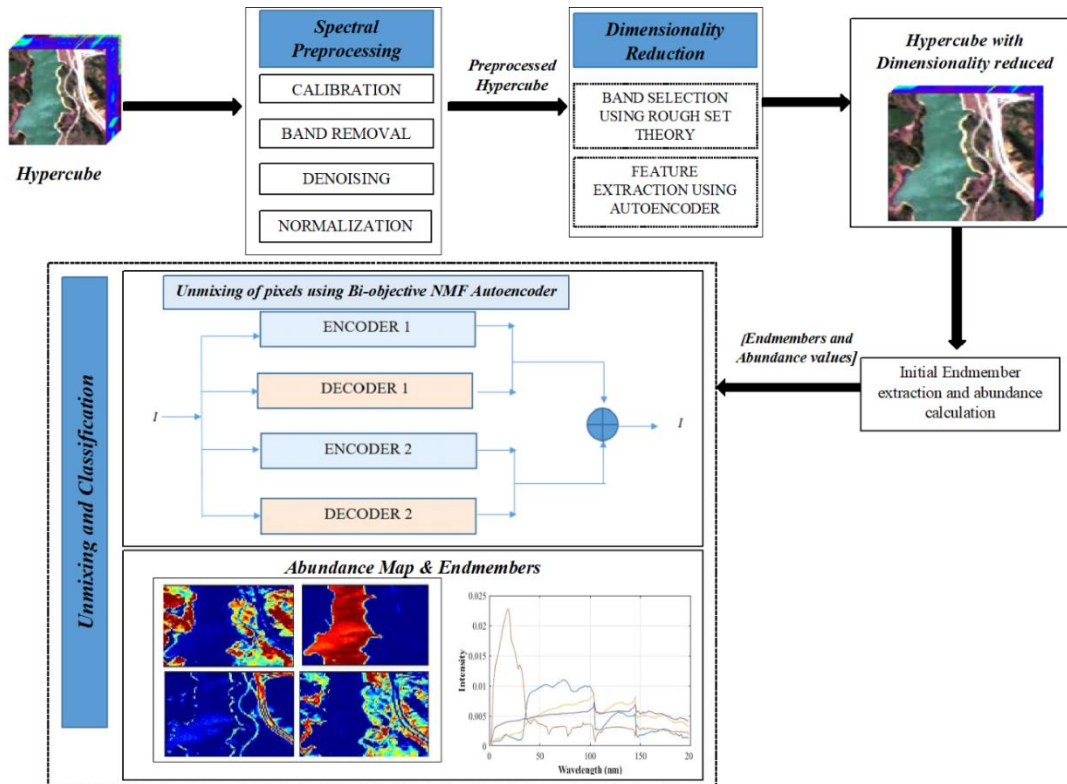


Figure 1. Proposed system architecture (NMF – BOA)

2.2. Dimensionality reduction

A single pixel in the Hypercube will be having millions of information. To reduce the computational complexity and to improve the performance of the classifier, dimensionality reduction is needed. The main dimensionality reduction methods for hyperspectral images are feature selection and feature extraction. In this model, rough set-based band selection is used for selecting the more informative bands and an autoencoder is used for feature extraction. For the band selection, the dependency value $\delta_{bi}(D)$ between the bands are calculated. Based on the dependency values, the redundant bands are removed and informative bands will be retained. The next dimensionality reduction is feature extraction. The classical models for feature extraction are principal component analysis (PCA), NMF, and independent component analysis (ICA). Recently many machine learning and deep learning methods have been proposed for feature extraction [25]. In our proposed model, the hypercube generated after band selection is given as the input to the autoencoder for the feature extraction. The autoencoder has two parts, the encoder, and the decoder. The image vector of the hypercube is represented as $I = [I_1, I_2, I_3, \dots, I_N] \in \mathbb{R}^{L \times N}$ where L is the number of Spectral bands and N is the number of Pixels. The encoder function in (3) is used for the feature extraction. And the image is reconstructed with reduced features using the decoder function in (4):

$$A = F(W_y + B_y) \tag{3}$$

$$D = F(W_d + B_d) \tag{4}$$

where W_y and B_y are the weight and bias for the activation function from the input layer to the hidden layer and W_d and B_d are the weight and bias for the activation function from the hidden layer to the output layer. The dimensionality reduction algorithm is given in Algorithm 1.

Algorithm 1. Dimensionality reduction (I)

1. Rough_Set_Band Selection (I_n)
 - i) Initialize New= $\{\Phi\}$ and Old= $\{b_1, b_2, b_3, \dots, b_k\}$
 - ii) for each b_i in Old find the dependency value $\delta_{b_i}(D)$ using the equation in Eq. (4)
 - iii) repeat steps iv, v until Old= $\{\Phi\}$
 - iv) select b_i with maximum dependency value $b_i = \arg \max_{b_i \in Old} \delta_{b_i}(D)$
 - v) New= $\{New \cup b_k\}$ Old= $\{Old - b_k\}$
2. Feature Extraction (I_n)
 - i) Feature extraction from the Hyperspectral image using the Encoder function
 $A = F(W_y + B_y)$
 - ii) Reconstruction of the output image using the decoder function.
 $I_D = F(W_d + B_d)$

2.3. Hyperspectral unmixing

Hyperspectral image unmixing or simply unmixing is the process of decomposing n multi-band observations $I=[I_1, \dots, I_n]$ into a collection of k individual spectra $M=[M_1, \dots, M_k]$, called endmembers, and calculating the fractional abundances $A=A_1, \dots, A_n$ [26]. Hyperspectral unmixing can be mainly classified into two, Linear mixture-based models [12], [27] and nonlinear mixture based models [26], [28], [29]. Endmember extraction is the process of identifying the pure pixels (also known as pure signatures) of a specific class.

2.3.1. Mixing model

If the mixture in the pixel is linear patches, then the model is called the LMM. On the other hand, if the mixture is complex and intimately mixed, then the model is called the NLMM. Linear mixing models are easy to implement, but in most real-time scenarios the mixtures are nonlinear. In this proposed model, a bilinear mixing model (BMM) is considered. The interactions are second order that is, the light scattered from one material can reflect off from another material and reach the sensor. If we consider two endmembers m_1 and m_2 , then the simple bilinear model can be defined as in (5):

$$I = m_1 \odot m_2 \tag{5}$$

where, \odot is the term-wise multiplication operator or Hadamard (term by term multiplication) operator. In the case of tissues, the light reflected from one tissue can be absorbed by nearby tissue and emit it later. So, the mixing will be nonlinear. So, to solve this, a nonlinear unmixing model is used.

2.3.2. Bi-objective nonlinear unmixing using NMF autoencoder (NMF-BOA)

NMF is a popular unmixing method used to extract the endmember and the abundance details together. Given a nonnegative matrix X which represents the hyperspectral image, we can find the matrix factors Y and Z based on classical nonnegative factorization as in (6).

$$X \approx YZ \tag{6}$$

Here, $X \in \mathbb{R}^{L \times N}$ is the hyperspectral image matrix with N pixels and L spectral bands. The matrix is factorized into $Y \in \mathbb{R}^{L \times R}$ which is the endmember matrix called the basis matrix, and $Z \in \mathbb{R}^{R \times N}$ the abundance or fraction matrix called the encoding matrix. There are several unmixing models proposed recently with good unmixing results for the nonlinear mixing model [10], [11]. In this proposed model, blind bilinear unmixing using NMF is implemented including the sparsity and regularization constraints [30]-[32]. Using the nonlinear mixing model, the (6) can be modified as (7).

$$I_D = EA + E_x A_x \tag{7}$$

where, $E_x A_x$ is the nonlinear term. But to unmix using NMF, the format of the equation needs to be as in (6). So, the terms are modified as (8)-(10).

$$E' = [E, E_x] \quad (8)$$

$$A' = [A, A_x] \quad (9)$$

$$I' = E'A' \quad (10)$$

For regularization, the sparsity terms are added. If the regularization is applied for the endmember term in (10) the mixing model becomes as in (11).

$$I_1' = E'A' + \alpha \|E\|_F \quad (11)$$

When the sparsity is added to both terms the equation will become as in (12).

$$I_2' = E'A' + \alpha \|E'\|_F + \beta \|A'\|_F \quad (12)$$

Where, F is the Frobenius/Hilbert-Schmidt norm and α and β are constants.

In our proposed model we are using two objective functions to implement nonnegative matrix factorization. The first objective function is designed from (11) and the second objective function is designed from (12) and is given in (13) and (14):

$$F_1(A', E') = \min_{E, A} \frac{1}{2} \|I - E'A'\|^2 + \alpha \|E'\|_F \quad (13)$$

$$F_2(A', E') = \min_{E, A} \frac{1}{2} \|I - E'A'\|^2 + \alpha \|E'\|_F + \beta \|A'\|_F \quad (14)$$

the (13) can be divided into two parts:

$$\min_{E'} \frac{1}{2} \|I - E'A'\|^2 + \alpha \|E'\|_F, \text{ st. } \sum A' = 1, A'_i \geq 0 \quad (15)$$

$$\min_{A'} \frac{1}{2} \|I - E'A'\|^2, \text{ st. } A'_i \geq 0 \quad (16)$$

same way the (14) can be divided into (17) and (18).

$$\min_{E'} \frac{1}{2} \|I - E'A'\|^2 + \alpha \|E'\|_F, \text{ st. } \sum A' = 1, A'_i \geq 0 \quad (17)$$

$$\min_{A'} \frac{1}{2} \|I - E'A'\|^2 + \beta \|A'\|_F, \text{ st. } A'_i \geq 0 \quad (18)$$

These objective functions are solved using the autoencoder designed motivated on [21]. The autoencoder pairs E1, E2, D1, and D2 are used to update the endmember and the abundance factors using the proximal decent approach. The encoder is designed using Algorithm 2 to update the endmember by fixing the Abundance and the decoder to update the Abundance by fixing endmember term. Here we are considering two objective functions and the final objective function as in (19) the value of $\lambda \in [0, 1]$. In this way, better-converged values can be considered.

$$\min_{A', E'} \lambda F_1(A', E') + (1 - \lambda) F_2(A', E') \quad (19)$$

Algorithm 2. Unmix(I_D, A, E)

- i) Initialize A and E
- ii) $I_D = EA + E_x A_x + n$
- iii) $E' = [E, E_x]$
- iv) $A' = [A, A_x]$
- v) $I' = E'A' + n$
- vi) $\min_{A', E'} \lambda F_1(A', E') + (1 - \lambda) F_2(A', E')$
- vii) While A and E converge
 - a. Fix $[E'_1, E'_2, E'_3, \dots, E'_M]$ and update A in Decoder
 - b. Fix $[A'_1, A'_2, A'_3, \dots, A'_M]$ and update E in Encoder
 - c. Normalize $[A'_1, A'_2, A'_3, \dots, A'_M]$ and $[E'_1, E'_2, E'_3, \dots, E'_M]$
 - d. Calculate $F([A'_1, A'_2, A'_3, \dots, A'_M], [E'_1, E'_2, E'_3, \dots, E'_M])$
- viii) Reconstruction of I

Here, the L1 and L2 sparsity norms are considered. The encoder is used for updating the abundance matrix and the decoder updates the endmember matrix. After the values are converged and satisfy the stopping criteria, the reconstructed image is produced.

2.3.3. Loss function

The root mean square error (RMSE) values are the loss functions used for the abundance values and are calculated by (20). The loss functions help the encoder to learn the required features. The spectral angular distance (SAD) is calculated using (21) and the total loss is calculated using (22).

$$RMSE(I', I) = \sqrt{\frac{1}{N} \sum_{i=1}^N \|a' - a\|^2} \tag{20}$$

$$SAD = \arccos \left(\frac{a'a}{\|a'\| \|a\|} \right) \tag{21}$$

$$Total Loss = l_1 RMSE + l_2 SAD \tag{22}$$

3. RESULTS AND DISCUSSION

In this section, the details of the datasets used and the results obtained are presented. For the performance comparison, the models TV-RSNMF [15], DAEN [19], and NMF-SAE [21] are considered. The performance analysis is done using RMSE and SAD defined in section 2.3.3

3.1. Experimental setup

The unmixing model was set up by SNR values from 20 dB to 35 dB. The number of pixels were 512×614 . The initial learning rates of the encoder and the decoder were set to 5×10^{-3} for the synthetic dataset and 6×10^{-3} for real dataset. 200 epochs were used for the training of the model. The learning rate was reduced by 15% after every 20 epochs. The l_1 and l_2 values in the total loss function are set to 5×10^3 and 6×10^{-3} .

3.1.1. Experiments on synthetic dataset

The spectral libraries provide the synthetic datasets. The dataset is created by endmember extraction and abundance calculation. The materials are selected from the United States Geological Survey (USGS) library and are selected as the endmembers. The abundance values are calculated and used for the performance evaluation.

3.1.2. Dataset description

Pure signals provided by the USGS library were considered for testing the performance of the model as in [1]. The materials considered were carnallite, Ammonijarosite, Almandine, Brucite, Axinite, and Chlorite. These materials are selected from the USGS library. The hyperspectral dataset contains 224 spectral bands. The wavelength ranges from 380 nm to 2500 nm.

3.1.3. Result obtained

The comparison of RMSE values with the standard deviation obtained for the synthetic dataset using the different models is illustrated in Table 1. The models considered for comparison are TV-RSNMF [15], DAEN [19], and NMF-SAE [21]. The proposed model achieved better performance for Ammonijarosite, Almandine, and Axinite compared to other models.

Table 1. RMSE values with standard deviation obtained for synthetic data

Algorithm	Carnallite	Ammonijarosite	Almandine	Brucite	Axinite	Chlorite
TV-RSNMF [15]	0.0691±4.16	0.1021±4.64	0.1128±7.03	0.0934±2.57	0.0972±2.95	0.0739±0.41
DAEN [19],	0.1082±3.94	0.1931±4.13	0.1292±1.02	0.1410±1.39	0.0844±4.45	0.0563±1.87
NMF-SAE [21]	0.0504±4.34	0.1034±5.71	0.0989±4.70	0.0908±4.77	0.0829±4.07	0.0772±6.41
NMF-BOA	0.0525±0.90	0.0913±4.11	0.0792±5.91	0.0972±4.48	0.0745±1.87	0.1013±1.86

3.2. Experiments with real dataset

Real-time datasets are different than synthetic datasets. The preprocessed techniques explained in section 2 are needed to be performed to make the real data to be suitable to perform the unmixing process. The details of the real dataset used in this model and the results obtained are presented in the following subsections.

3.2.1. Dataset description

The dataset used for the analysis of the proposed model is the Jasper Ridge dataset. It is a popular real dataset used for the unmixing analysis in many software like ENVI. The sample Jasper Ridge dataset is shown in Figure 2. The synthetic red green blue (RGB) image of the hyperspectral image is given in Figure 2(a) and the classification map is given in Figure 2(b). The dataset contains 512×624 -pixel hyperspectral images captured using 224 channels of electromagnetic spectrum in the range of 380 nm to 2500 nm with a spectral resolution of 9.46 nm. In our proposed model we use four endmembers for the Jasper dataset which are tree, water, soil, and road. Since the whole hyperspectral image is too complex to process, a part of it with 100×100 pixels (the sub-image starts at the pixel position (105,269)). The number of channels is also reduced by band removal. The band ranges from 1 to 3, 108 to 112, 154 to 166, and 220 to 224 are removed, and the remaining 198 channels are considered. The hyperspectral image is preprocessed by removing water absorption and other calibrations. The spectral reflectance of the endmember is depicted in Figure 3. The ground truth is given in Figure 3(a) and the obtained endmember spectra are given in Figure 3(b). After the dimensionality reduction which includes band selection and feature extraction, a total of 60 informative bands are considered in this model.

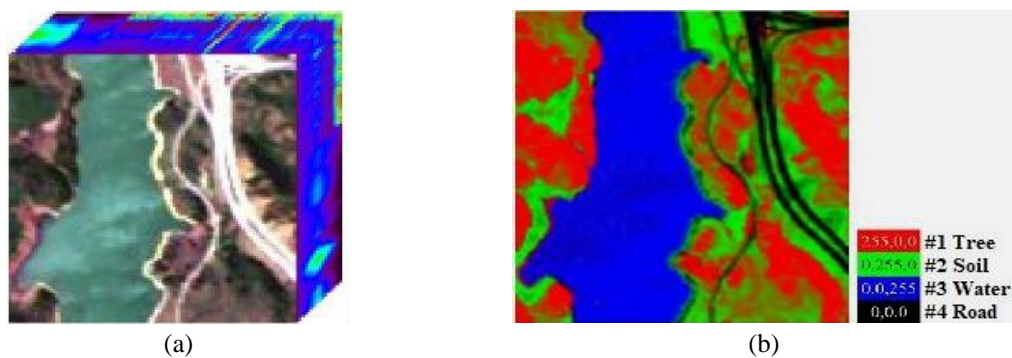


Figure 2. Jasper ridge dataset (a) original dataset and (b) classification map

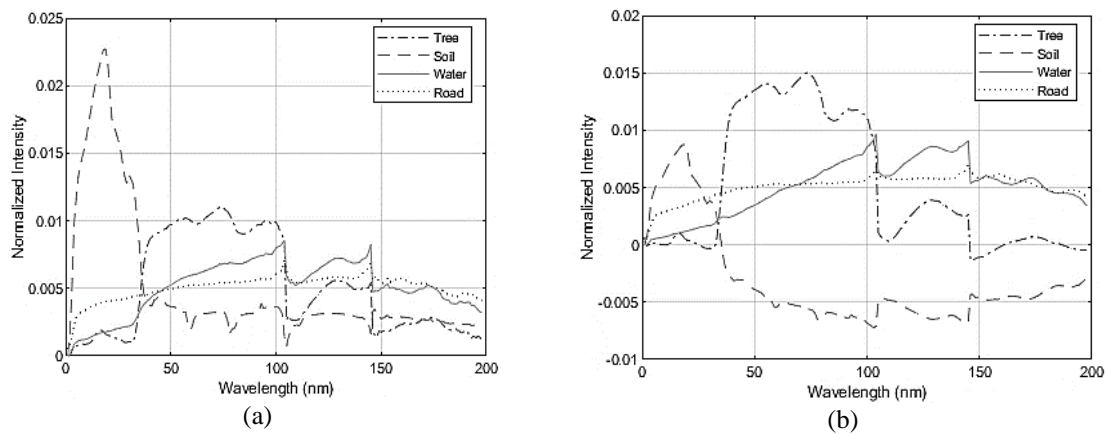


Figure 3. The endmembers (a) ground truth (b) extracted endmembers

3.2.3. Results obtained

In this section, the performance analysis of our model and the comparative analysis with the existing models are given. RMSE and SAD values obtained are given in Table 2. The models considered for the comparison are the TV-RSNMF [15], DAEN [19], and NMF-SAE [21]. The results show that our proposed model achieved better performance for the endmembers of the tree, soil, water, and road are compared to the existing models. The abundance map generated using our model and the state-of-the-art models are given in Table 3. The results of endmember extraction are illustrated in Figure 3. The ground truth and endmembers extracted using our model are given in Figures 3(a) and 3(b) respectively. The comparison of mean RMSE values is illustrated in Figure 4.

Table 2. RMSE values obtained for different SNR values

Algorithm	PSNR	Tree	Water	Soil	Road
TV-RSNMF [15]	20 dB	0.0716±5.70	0.0982±0.98	0.1529±3.15	0.1881±2.55
	25 dB	0.07092±4.50	0.1010±0.34	0.2092±2.91	0.1530±3.24
	30 dB	0.0696±0.71	0.1217±0.84	0.1289±3.82	0.1810±4.12
	35 dB	0.0711±6.56	0.0928±0.90	0.1485±3.43	0.1572±1.95
DAEN [19]	20 dB	0.0932±2.38	0.1029±0.61	0.1081±3.45	0.0862±3.18
	25 dB	0.0963±5.40	0.0973±0.70	0.1102±3.92	0.0781±2.44
	30 dB	0.08936±4.72	0.1081±0.68	0.1093±3.83	0.0798±3.26
	35 dB	0.0992±2.20	0.0482±0.52	0.1023±2.94	0.0821±2.97
NMF-SAE [21]	20 dB	0.0494±1.90	0.0629±0.50	0.0527±4.17	0.0932±0.57
	25 dB	0.0513±2.39	0.0982±0.18	0.0512±2.34	0.0972±2.55
	30 dB	0.0458±1.72	0.0982±0.78	0.0498±4.56	0.2340±2.55
	35 dB	0.0529±5.60	0.0982±0.21	0.0434±2.34	0.1032±2.55
NMF-BOA	20 dB	0.0518±0.90	0.0511±0.61	0.0760±1.98	0.0545±0.58
	25 dB	0.0523±5.81	0.0620±0.12	0.0782±3.15	0.0682±1.45
	30 dB	0.0612±1.40	0.0721±0.91	0.0412±3.52	0.0881±2.38
	35 dB	0.0434±4.32	0.0589±0.73	0.0627±3.49	0.0734±0.65

Table 3. Abundance map comparison

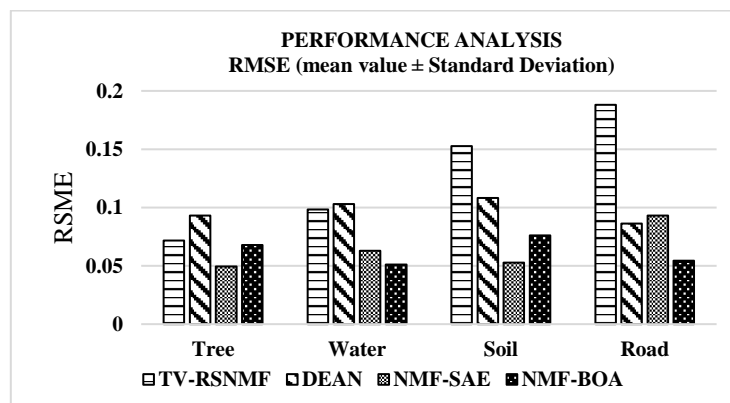
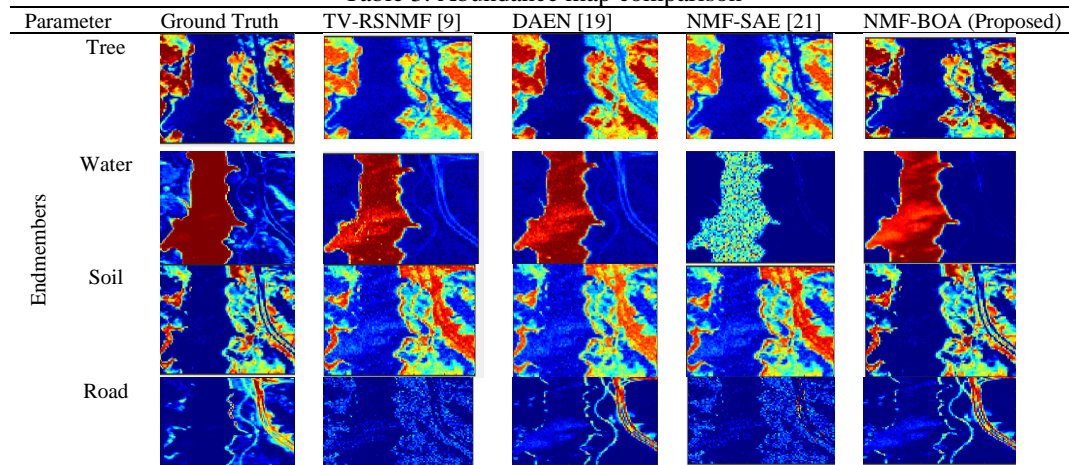


Figure 4. Comparison of mean RMSE values

4. CONCLUSION

Hyperspectral images are captured in long ranges of continuous electromagnetic spectra and one single pixel may contain millions of information. Due to many atmospheric and sensor conditions, a single pixel may include information about more than one material. Hyperspectral unmixing is one of the emerging tools for improving hyperspectral image classification and prediction analysis by solving the mixed pixel problem. The mixture of materials present in the observing scene can be a linear combination or a nonlinear combination. The real-world images are not always in a linear mixture. So, a better nonlinear unmixing model for real-world scenarios is required. In this proposed model a bi-objective autoencoder system named NMF-

BOA is used for the unmixing of hyperspectral images using a modified nonlinear mixing model. The analysis shows that although noise in the real dataset is a limitation, better performance is achieved compared to the existing unmixing models. Aims for future work include better optimization and time complexity improvement.





REFERENCES

- [1] M. S. Navin and L. Agilandeewari, "Multispectral and hyperspectral images based land use / land cover change prediction analysis: an extensive review," *Multimedia Tools and Applications*, vol. 79, no. 39–40, pp. 29751–29774, 2020, doi: 10.1007/s11042-020-09531-z.
- [2] M. Prabukumar, S. Sawant, S. Samiappan, and L. Agilandeewari, "Three-dimensional discrete cosine transform-based feature extraction for hyperspectral image classification," *Journal of Applied Remote Sensing*, vol. 12, no. 04, p. 1, 2018, doi: 10.1117/1.jrs.12.046010.
- [3] S. S. Sawant, P. Manoharan, and A. Loganathan, "Band selection strategies for hyperspectral image classification based on machine learning and artificial intelligent techniques –Survey," *Arabian Journal of Geosciences*, vol. 14, no. 7, 2021, doi: 10.1007/s12517-021-06984-w.
- [4] S. S. Sawant, M. Prabukumar, A. Loganathan, F. A. Alenzi, and S. Ingaleswar, "Multi-objective multi-verse optimizer based unsupervised band selection for hyperspectral image classification," *International Journal of Remote Sensing*, vol. 43, no. 11, pp. 3990–4024, Jun. 2022, doi: 10.1080/01431161.2022.2105666.
- [5] A. L. P. M, and S. R. S, "An efficient hybrid approach for hyperspectral image classification," *International Journal of Pure and Applied Mathematics*, vol. 117, no. 17, pp. 135–141, 2017.
- [6] G. Tejasree and L. Agilandeewari, "Gradient Boosting ensemble method for in-vivo brain tumour classification using hyperspectral images," *Indian Journal of Computer Science and Engineering*, vol. 13, no. 5, pp. 1660–1672, 2022, doi: 10.21817/indjcs/2022/v13i5/221305179.
- [7] L. Agilandeewari, M. Prabukumar, V. Radhesyam, K. L. N. B. Phaneendra, and A. Farhan, "Crop classification for agricultural applications in hyperspectral remote sensing images," *Applied Sciences (Switzerland)*, vol. 12, no. 3, 2022, doi: 10.3390/app12031670.
- [8] D. D. Lee and H. S. Seung, "Algorithms for non-negative matrix factorization," *Advances in Neural Information Processing Systems*, no. 1, 2001.
- [9] K. Qu, W. Bao and X. Shen, "Hyperspectral unmixing using weighted $l_{1/2}$ sparse total variation regularized and volume prior constrained nonnegative matrix factorization," *IGARSS 2019 - IEEE International Geoscience and Remote Sensing Symposium*, Yokohama, Japan, 2019, pp. 2147–2150, doi: 10.1109/IGARSS.2019.8898830.
- [10] X. Zhang, Y. Sun, J. Zhang, P. Wu, and L. Jiao, "Hyperspectral unmixing via deep convolutional neural networks," *IEEE Geoscience Remote Sensing Letters*, vol. 15, no. 11, pp. 1755–1759, 2018, doi: 10.1109/LGRS.2018.2857804.
- [11] B. Palsson, J. Sigurdsson, J. R. Sveinsson, and M. O. Ulfarsson, "Hyperspectral unmixing using a neural network autoencoder," *IEEE Access*, vol. 6, pp. 25646–25656, 2018, doi: 10.1109/ACCESS.2018.2818280.
- [12] F. Z. Benhalouche, Y. Deville, M. S. Karoui, and A. Ouamri, "Hyperspectral unmixing based on constrained bilinear or linear-quadratic matrix factorization," *Remote Sensing*, vol. 13, no. 11, 2021, doi: 10.3390/rs13112132.
- [13] W. Wang, Y. Qian, and H. Liu, "Multiple clustering guided nonnegative matrix factorization for hyperspectral unmixing," *IEEE Journal of Selected Topics in Applied Earth Observations and Remote Sensing*, vol. 13, pp. 5162–5179, 2020, doi: 10.1109/JSTARS.2020.3020541.
- [14] C. Peng, Y. Zhang, Y. Chen, Z. Kang, C. Chen, and Q. Cheng, "Log-based sparse nonnegative matrix factorization for data representation," *Knowledge Based Systems*, vol. 251, pp. 109127, 2022, doi: 10.1016/j.knsys.2022.109127.
- [15] W. He, H. Zhang, and L. Zhang, "Total variation regularized reweighted sparse nonnegative matrix factorization for hyperspectral unmixing," *IEEE Transactions on Geoscience and Remote Sensing*, vol. 55, no. 7, pp. 3909–3921, 2017, doi: 10.1109/TGRS.2017.2683719.
- [16] F. Xiong, Y. Qian, J. Zhou, and Y. Y. Tang, "Hyperspectral unmixing via total variation regularized nonnegative tensor factorization," *IEEE Transactions on Geoscience and Remote Sensing*, vol. 57, no. 4, pp. 2341–2357, 2019, doi: 10.1109/TGRS.2018.2872888.
- [17] S. Zhang *et al.*, "Spectral-spatial hyperspectral unmixing using nonnegative matrix factorization," *IEEE Transactions on Geoscience and Remote Sensing*, vol. 60, 2022, doi: 10.1109/TGRS.2021.3074364.
- [18] L. Dong, X. Lu, G. Liu, and Y. Yuan, "A novel NMF guided for hyperspectral unmixing from incomplete and noisy data," *IEEE Transactions on Geoscience and Remote Sensing*, vol. 60, 2022, doi: 10.1109/TGRS.2021.3101504.
- [19] Y. Su, J. Li, A. Plaza, A. Marinoni, P. Gamba, and S. Chakravorty, "DAEN: deep autoencoder networks for hyperspectral unmixing," *IEEE Transactions on Geoscience and Remote Sensing*, vol. 57, no. 7, pp. 4309–4321, 2019, doi: 10.1109/TGRS.2018.2890633.
- [20] A. Min and H. Li, "A probability metric-based autoencoder for hyperspectral unmixing," *IEEE Transactions on Geoscience and Remote Sensing*, vol. 60, 2022, doi: 10.1109/TGRS.2021.3131773.
- [21] F. Xiong, J. Zhou, M. Ye, J. Lu and Y. Qian, "NMF-SAE: An interpretable sparse autoencoder for hyperspectral unmixing," *ICASSP 2021 - 2021 IEEE International Conference on Acoustics, Speech and Signal Processing (ICASSP)*, Toronto, ON, Canada, 2021, pp. 1865–1869, doi: 10.1109/ICASSP39728.2021.9414084.
- [22] Z. Dou, K. Gao, X. Zhang, H. Wang, and J. Wang, "Blind hyperspectral unmixing using dual branch deep autoencoder with orthogonal sparse prior," *ICASSP, IEEE International Conference on Acoustics, Speech and Signal Processing (ICASSP) - Proc.*, vol. 2020-May, 2020, pp. 2428–2432, doi: 10.1109/ICASSP40776.2020.9053341.
- [23] Q. Jin, Y. Ma, F. Fan, J. Huang, X. Mei, and J. Ma, "Adversarial autoencoder network for hyperspectral unmixing," *IEEE Transactions on Neural Networks and Learning Systems*, vol. 18, no. 9, pp. 1640–1644, 2021, doi: 10.1109/TNNLS.2021.3114203.
- [24] O. Eches and M. Guillaume, "A bilinear-bilinear nonnegative matrix factorization method for hyperspectral unmixing," *IEEE Transactions on Geoscience and Remote Sensing*, vol. 11, no. 4, pp. 778–782, 2014, doi: 10.1109/LGRS.2013.2278993.
- [25] S. Ding, C. A. Keal, L. Zhao, and D. Yu, "Dimensionality reduction and classification for hyperspectral image based on robust supervised ISOMAP," *Journal of Industrial and Production Engineering*, vol. 39, no. 1, pp. 19–29, 2022, doi: 10.1080/21681015.2021.1952657.
- [26] C. Févotte and N. Dobigeon, "Nonlinear hyperspectral unmixing with robust nonnegative matrix factorization," *IEEE Transactions on Image Processing*, vol. 24, no. 12, pp. 4810–4819, 2015, doi: 10.1109/TIP.2015.2468177.





- [27] A. Gómez-Sánchez *et al.*, “Linear unmixing protocol for hyperspectral image fusion analysis applied to a case study of vegetal tissues,” *Scientific Reports*, vol. 11, no. 1, pp. 1–14, 2021, doi: 10.1038/s41598-021-98000-0.
- [28] J. Gu, B. Yang, and B. Wang, “Nonlinear unmixing for hyperspectral images via kernel-transformed bilinear mixing models,” *IEEE Transactions on Geoscience and Remote Sensing*, vol. 60, 2022, doi: 10.1109/TGRS.2021.3135571.
- [29] X. Tao *et al.*, “Fast orthogonal projection for hyperspectral unmixing,” *IEEE Transactions on Geoscience and Remote Sensing*, vol. 60, 2022, doi: 10.1109/TGRS.2022.3150263.
- [30] Z. Li, Y. Altmann, J. Chen, S. McLaughlin, and S. Rahardja, “Sparse linear spectral unmixing of hyperspectral images using expectation-propagation,” *IEEE Transactions on Geoscience and Remote Sensing*, vol. 60, pp. 1–13, 2022, doi: 10.1109/TGRS.2022.3147423.
- [31] G. Wang, Y. Zhang, W. F. Xie, Y. Qu, and L. Feng, “Hyperspectral linear unmixing based on collaborative sparsity and multi-band non-local total variation,” *International Journal of Remote Sensing*, vol. 43, no. 1, pp. 1–26, 2022, doi: 10.1080/01431161.2021.1996653.
- [32] Y. Miao and B. Yang, “Sparse unmixing for hyperspectral imagery via comprehensive-learning-based particle swarm optimization,” *IEEE Journal of Selected Topics in Applied Earth Observations and Remote Sensing*, vol. 14, pp. 9727–9742, 2021, doi: 10.1109/JSTARS.2021.3115177.

BIOGRAPHIES OF AUTHORS







Sreejam Muraleedhara Bhakthan     is pursuing her Ph.D. at the School of Information Technology and Engineering, VIT Vellore. She completed her Bachelor of Technology in Computer Science and Engineering in the year 2014 (under Cochin University of Science and Technology (CUSAT)) and Master of Technology in the year 2017 (APJ Abdul Kalam Technological University (KTU)) from the College of Engineering Perumon, Kollam, Kerala, India. She worked as a Guest Lecturer in Govt. Polytechnic Punalur, Kollam, and as Assistant Professor in Vidya Academy of Science and Technology Technical Campus Kilimanoor, Trivandrum. Her areas of interest include image processing, machine learning, and remote sensing. She can be contacted by email: sreejam.m2020@vitstudent.ac.in.



Agilandeewari Loganathan     completed her Ph.D. and working as a Professor in the Department of Software Systems and Engineering, School of Information Technology and Engineering (SITE), VIT Vellore. She received her Bachelor's degree in Information Technology and Master's in Computer Science and Engineering from Anna University in 2005 and 2009 respectively. She is having around 14+ years of teaching experience and published 50+ papers in peer-reviewed reputed journals. Her reputed publications include research articles in peer-reviewed journals namely expert systems with applications, IEEE Access, Journal of Ambient Intelligence and Humanized Computing, Multimedia Tools and Applications, and Journal of Applied Remote Sensing indexing at Thomson Reuters with an average impact factor of 5. She is a peer reviewer in journals including IEEE Access, Pattern Recognition, International Journal of Remote Sensing, Array, Artificial Intelligence Review, Informatics in Medicine Unlocked, Neurocomputing, Computers, and Electrical Engineering, Journal of King Saud University-Computer and Information Sciences, IET Review, and Journal of Engineering Science and Technology (JESTEC). She also published about 13 engineering books as per Anna University Syllabus. She is a lifetime member of the Computer Society of India. Her areas of interest include image and video watermarking, image processing, neural networks, cryptography fuzzy logic, machine learning, IoT, information-centric networks, and remote sensing. She can be contacted by email: agila.l@vit.ac.in.



Aashish Bansal     is pursuing his B.Tech. at the School of Information Technology and Engineering, Vellore Institute of Technology, Vellore. He is working as Academic Intern Tech at Bank of America Continuum India since January 2023. His research interest includes digital image and video processing, artificial intelligence, machine learning, deep learning, digital forensics, and network and information security. He can be contacted by email: aashish.bansal2019@vitstudent.ac.in.